8352–8367 *Nucleic Acids Research, 2015, Vol. 43, No. 17* *Published online 3 August 2015*
doi: 10.1093/nar/gkv754

ATM-dependent phosphorylation of MRE11 controls extent of resection during homology directed repair by signalling through Exonuclease 1

Amanda W. Kijas[1], Yi Chieh Lim[2], Emma Bolderson[3], Karen Cerosaletti[4], Magtouf Gatei[1], Burkhard Jakob[5], Frank Tobias[5], Gisela Taucher-Scholz[5], Nuri Gueven[6], Greg Oakley[7], Patrick Concannon[8], Ernst Wolvetang[9], Kum Kum Khanna[10], Lisa Wiesmüller[11] and Martin F. Lavin[1,*]

[1]The University of Queensland, UQ Centre for Clinical Research, University of Queensland, Brisbane, Queensland 4029, Australia, [2]Brain Cancer Research Unit, QIMR Berghofer Medical Research Institute, Brisbane, Queensland 4029, Australia, [3]Genome Stability Laboratory, Translational Research Institute, Queensland University of Technology, Queensland 4102, Australia, [4]Translational Research Program, Benaroya Research Institute, Seattle, WA 981010, USA, [5]GSI Helmholtzzentrum für Schwerionenforschung, Darmstadt 64291, Germany, [6]School of Medicine, Faculty of Health, University of Tasmania, Hobart, Tasmania 7001, Australia, [7]University of Nebraska College of Dentistry, Lincoln, NE 68583-0740, USA, [8]Genetics Institute, University of Florida, Gainesville, Florida, FL 3261, USA, [9]Australian Institute for Bioengineering and Nanotechnology, University of Queensland, Brisbane 4072, Australia, [10]Signal transduction, QIMR Berghofer Medical Research Institute, Brisbane, Queensland 4029, Australia and [11]Department of Obstetrics and Gynaecology, University of Ulm, Ulm 89075, Germany

Received June 13, 2014; Revised July 10, 2015; Accepted July 14, 2015

ABSTRACT

The MRE11/RAD50/NBS1 (MRN) complex plays a central role as a sensor of DNA double strand breaks (DSB) and is responsible for the efficient activation of ataxia-telangiectasia mutated (ATM) kinase. Once activated ATM in turn phosphorylates RAD50 and NBS1, important for cell cycle control, DNA repair and cell survival. We report here that MRE11 is also phosphorylated by ATM at S676 and S678 in response to agents that induce DNA DSB, is dependent on the presence of NBS1, and does not affect the association of members of the complex or ATM activation. A phosphosite mutant (MRE11S676AS678A) cell line showed decreased cell survival and increased chromosomal aberrations after radiation exposure indicating a defect in DNA repair. Use of GFP-based DNA repair reporter substrates in MRE11S676AS678A cells revealed a defect in homology directed repair (HDR) but single strand annealing was not affected. More detailed investigation revealed that MRE11S676AS678A cells resected DNA ends to a greater extent at sites undergoing HDR. Furthermore, while ATM-dependent phosphorylation of Kap1 and SMC1 was normal in MRE11S676AS678A cells, there was no phosphorylation of Exonuclease 1 consistent with the defect in HDR. These results describe a novel role for ATM-dependent phosphorylation of MRE11 in limiting the extent of resection mediated through Exonuclease 1.

INTRODUCTION

Exposure of cells to DNA damage leads to a variety of lesions of which DNA double strand breaks (DSB) represent the greatest threat to the integrity and survival of cells (1). In mammalian cells these DSB are repaired primarily by non-homologous end joining (NHEJ) and homologous recombination (HR). However, alternative pathways such as microhomology-mediated end joining (MMEJ) and single strand annealing (SSA) pathways also contribute to repair of DNA DSB. Of these the major pathway is NHEJ, which occurs throughout the cell cycle, requiring the Ku70/80 heterodimer and the catalytic subunit of DNA-dependent protein kinase (DNA-PKcs) to initiate the process of DNA DSB repair (2). The activated holoenzyme phosphorylates itself and other substrates to complete the process of repair (3). The availability of sister chromatids in S and G2 phases enables repair using HR but pathway choice is also influenced by DNA-PKcs acting in concert with MRE11/RAD50/NBS1 (MRN) (3), recruitment of the MRN complex to DNA DSB by single-stranded bind-

*To whom correspondence should be addressed. Tel: +61 7 33466045; Fax: +61 7 33465599; Email: m.lavin@uq.edu.au

ing protein (hSSB1) (4), cyclin-dependent kinase (CDK) phosphorylation of NBS1 and the opposing activities of 53BP1/RIF1 and BRCA1/CtIP (5,6). Resection of DNA 5′ ends at the DSB gives rise to 3′ single strand DNA which is required for RAD51 binding and initiation of HR (7). The MRN complex is required for the generation of 5′ resected ends, where MRE11's endonuclease activity has been shown to nick the DNA upstream from the break then resect 3′→5′ towards the break, followed by more extensive resection by two independent nucleases, Exonuclease 1 and Dna 2 (8–12). This was more carefully dissected in mammalian cells by Shibata *et al.* (12) where they used specific inhibitors for endonuclease versus exonuclease acitivites of MRE11 and found that the inhibition of MRE11's endonuclease activity promoted NHEJ, thus a key step in resection enabling Exonuclease 1 access to the DNA substrate. Another protein CtIP acts cooperatively with the MRN complex to enhance resection and HR (13).

The MRN complex functions both in the recognition and processing of DNA DSB, to signal these to cellular processes involved in enhancing cell survival (14). Mutations in genes encoding for members of the complex give rise to ataxia-telangiectasia-like disorder (ATLD), Nijmegen breakage syndrome (NBS) and NBS-like disorder (15–17). While these are distinct syndromes they show overlap in cellular phenotype which includes radiosensitivity, cell cycle defects and a defective response to DNA damage (18,19). An early event in the response to DNA damage is the localization of MRN to the DNA DSB (18,19). The complex acts as a molecular clamp at the DNA DSB (20), facilitates local DNA unwinding and participates in DNA resection as described above (21). Once in place, MRN recruits the kinase, ataxia-telangiectasia mutated (ATM) to the DNA DSB where it is activated by acetylation and autophosphorylation (22–24). Once activated, ATM phosphorylates a multitude of substrates involved in cell cycle control, DNA repair, cell survival and other cellular processes (25). Members of the MRN complex are also phosphorylated by ATM to play an adaptor role in phosphorylation of downstream substrates (26,27) ATM-dependent phosphorylation of NBS1 regulates the S phase checkpoint (26,28) as well as controlling its accumulation and that of ATM at sites of DNA DSB (29). This phosphorylation has also been reported to play a role in cell survival post-irradiation (30,31). NBS1 is also phosphorylated by CDK which stimulates the conversion of DNA DSB into structures that are substrates for HR repair (6). A second member of the complex, RAD50, is phosphorylated at a single site (S635) by ATM in response to DNA DSB (27). This phosphorylation is important for ATM-dependent signalling through SMC1 for DNA repair and cell cycle checkpoint control in maintaining genome integrity. Five other RAD50 phosphorylations have been identified in phosphoproteomic analysis but these have not been assigned to specific protein kinases (32–34).

Phosphoproteomic analysis has also identified several phosphorylation sites on MRE11 (32,34,35). Matsuoka *et al.* (32) identified a single MRE11 phosphorylation site (S678) and Bennetzen *et al.* (35) identified multiple sites (including S676, S678 and S681), where the S676 and S678 sites were present in an ATM consensus SQSQ sequence. Previous studies have shown that MRE11 is hyperphosphorylated in response to the treatment of cells with a variety of genotoxic agents, including gamma irradiation (36,37). There is also evidence that this phosphorylation is ATM-dependent in response to DNA damage (38,39). However, in both of the latter studies phosphorylation was detected as a mobility shift of a fraction of the protein at high radiation doses and no specific sites were identified. A more recent study using *Xenopus* extracts narrowed putative phosphorylation sites to a small region of ATM consensus sites (SQ/TQ) within the C-terminus of MRE11 again observed as a migration shift (40). They went on to show that the hyperphosphorylation of MRE11 inactivated the MRN complex by facilitating its disassociation from chromatin, allowing for down regulation of the DNA damage signalling during cell cycle checkpoint recovery following DNA repair. Thus while specific sites of ATM-dependent phosphorylation and linked functional activity are described for NBS1 and RAD50 the picture is less clear for MRE11.

Here we show that ATM phosphorylates MRE11 on two adjacent sites, acting as the controlling switch to restrict the extent of resection by Exonuclease 1 at any particular site during homology directed repair. We demonstrate that these phosphorylation sites are functionally important for repair of DNA damage and subsequent cell survival.

MATERIALS AND METHODS

Plasmid constructs

Full length MRE11 was sub-cloned from pACT2 MRE11 plasmid clone (41), into pLXIN (to create pLXINWT) retroviral vector (Clontech) then the Quick Change Site-Directed Mutagenesis kit (Stratagene) was used to create the MRE11S676AS678A mutant (ATLD-MUT). MRE11 cloned into pEYFP-C1 was kindly provided by Jean-Yves Masson (42), and the alanine MRE11S676AS678A mutant (non-phosphorylatable) and aspartic acid MRE11S676DS678D (phosphomimetic) mutants were made using site directed mutagenesis and sequence confirmed.

Cell lines

Lymphoblastoid control (C2ABR, C3ABR), A-T (AT1ABR), NBS (NBS03) and ATLD2 (B8731) cell lines were grown in 1640 RPMI supplemented with 10% foetal calf serum, penicillin (100 μg/ml) and streptomycin (100 μg/ml). Fibroblast control (NFF), A-T (AT4BI) and the human osteosarcoma cells, U2OS were grown in Dulbecco's modified Eagle's medium (DMEM) supplemented with 10–12% foetal calf serum, penicillin (100 μg/ml) and streptomycin (100 μg/ml). Using the pLXIN series of vectors from above, stable cell lines were created in ATLD2hT cells (D6809), kindly provided by S. Jackson. Creating VEC (using pLXIN), MUT (using pLXINMRE11S676AS678A), WT (pLXINMRE11) as well as S676A (pLXINMRE11S676A) and S678A (pLXINMRE11S678A) cell lines. These stably transfected lines were grown in DMEM supplemented with 15% foetal calf serum, 250 μg/ml G418, penicillin (100 μg/ml) and

streptomycin (100 μg/ml). All cells were grown at 37°C with 5% CO_2.

The preparation and use of MRE11S676S678 and MRE11pS676pS678 rabbit antibody

Serum was raised in rabbits (Institute of Medical and Veterinary Science, Australia), against the phospho-peptide SKIM(pS)Q(pS)QVSC synthesized by Mimotopes (Australia). Then both the unphosphorylated and phosphorylated peptides were crosslinked to Sulfolink resin (Pierce) for subsequent antibody affinity chromatography. Purified antibody was used to precipitate MRE11 from total cell extracts prepared in cell lysis buffer (50 mM Tris pH 7.4, 100 mM NaCl, 1 mM EDTA, 1 mM EGTA 0.2% Triton X-100, 0.3% IGEPAL CA-630, 25 mM β-glycerophosphate, 1 mM dithiothreitol (DTT), 10 mM Na_3VO_4, 10 mM sodium fluoride and 1× Complete protease inhibitor (Roche Diagnostics)). Immunoprecipitations were performed o/n at 4°C in the same buffer but 0.1% Triton X-100, 0.15% IGEPAL CA-630 and 12.5 mM β-glycerophosphate.

Lysate preparations, co-immunoprecipitations and western blot analysis

We exposed control, A-T and NBS lymphoblastoid cell lines to varying doses of gamma irradiation and collected them at the time points indicated. Total cell extracts were prepared by using cell lysis buffer (50 mM Tris pH 7.4, 0.15 M NaCl, 10% Glycerol, 0.5% Tween 20, 50 mM β-glycerophosphate, 1 mM DTT, 1 mM PMSF, 5–10 μg/ml Aprotinin, 5 μg/ml Leupeptin, 5 μg/ml Pepstatin, 1mM Na_3VO_4, 1 mM NaF). MRE11 immunoprecipitations were performed using anti-MRE11 antibody (Novus). Whole cell extracts or immune complexes were separated by electrophoresis on sodium dodecyl sulphate-polyacrylamide gel electrophoresis (SDS-PAGE) gels and proteins transferred to nitrocellulose membranes using Towbin's buffer (20% methanol, 50 mM Tris, 40 mM glycine and 0.02% SDS) at 100 V for 1 h. Blots were incubated with antibodies against MRE11 (12D7; GeneTex), Phospho-SQ/TQ (Cell Signaling Technologies), RAD50 (Upstate), NBS1 (Novus Biologicals), ATM (2C1; GeneTex), ATM pS1981 (GeneTex), SMC1 and SMC1 pS957 (GeneTex), Kap1 and Kap1 p824 (Novus Biologicals), GAPDH (GeneTex) and GFP (Abcam).

Kinase assay

Three GST-MRE11 constructs spanning the full-length of MRE11, GST-MRE11A:1–273 aa, GST-MRE11B:223–525 aa and GST-MRE11C:487–708 aa (Figure 1C) were cloned. Serines-531, 590, 676 and 678 of GST-MRE11C were substituted with alanine using the Quick Change Site-Directed Mutagenesis kit according to the manufacturer's directions (Stratagene). Anti-ATM immunoprecipitates (ATM-5BA antibody) from control and A-T cells that were treated with 10 Gy of ionizing radiation (IR) were incubated in kinase buffer (10 mM Hepes, pH 7.5, 50 mM β-glycerophosphate, 50 mM NaCl, 10 mM $MgCl_2$, 10 mM $MnCl_2$, 1 mM DTT, 5 mM adenosine triphosphate (ATP), 10 μCi [γ-32P] ATP and 1 μg of MRE11 protein) for 30 min at 30°C and analysed by SDS-PAGE, followed by autoradiography.

Clonogenic cell survival assay

Cells were irradiated with 0, 1, 2, 3, 4 or 5 Gy then plated out and surviving cells grown to form colonies, these were stained with crystal violet. The mean from three independent experiments was plotted with the standard deviation as percent survival.

Induced-chromosome aberrations

Cells were irradiated then 0.1 μg/ml colcemid was added immediately post-irradiation. The cells were harvested 12 h later (G2 cells) and treated for 15 min in 0.075 M potassium chloride then fixed in methanol-glacial acetic acid (3:1) and spread on glass slides. The cells were then stained with Giemsa and 50 metaphases were analysed for each sample.

Carbon and Uranium ion irradiation and YFP-MRE11 recruitment

U2OS cells were transiently transfected with pEYFP-MRE11 (WT), MRE11S676AS678A (MUT), MRE11S676DS678D (DD), MRE11S676A (S676A) or MRE11S678A (S678A) plasmids respectively using electroporation (Amaxa Nucleofector, Germany) 24 h prior to irradiation. Charged particle irradiation was done at the UNILAC accelerator at GSI using 9.8 MeV/u carbon ions (LET 170 keV/μm) or 4.7 MeV/u uranium ions (LET 15000 keV/μm) under a low angle as described previously (43). Cells were fixed with 2% paraformaldehyde unirradiated or 10 min, 1, 4 or 12 h post-irradiation. Immunostaining with γH2AX (Millipore) was done according to Jakob *et al.* (44). DNA was counterstained with 1 μg per ml DAPI. Microscopic imaging was performed using a spinning disc confocal microscope (Nikon Eclipse Ti with Yokogawa CSU_X1) utilizing a Plan APO 100 × 1.4 NA oil immersion lens or a Leica SPE laser scanning confocal (Planapo 63× 1.3 NA). Optical sections were recorded in increments of 300 μm across the thickness of cells. The total magnification of the systems yielded pixels corresponding to 72 × 72 nm in lateral dimensions. Real time recruitment kinetics of wild-type (WT) and mutant YFP-MRE11 after carbon or uranium ion irradiation was evaluated using the GSI beamline microscope as described previously (45). About 32 to 55 nuclei were analysed for each plasmid (8 samples for each condition).

Double strand break repair GFP reporter assays

The cell lines ATLDWT, ATLDS676AS678A and ATLD-VEC were transiently transfected (1.5×10^5 cells) using a 10 μl NEON (Life Technologies), electroporation tip (1400 V, 20 ms and 2 pulses). The DNA repair substrate plasmids (0.5 μg) used to assess HR (pHR-EGFP/5′EGFP), microhomology-mediated NHEJ (pEJ-EGFP) and SSA (p5′EGFP/HR-EGFP) were co-transfected with 1 μg of

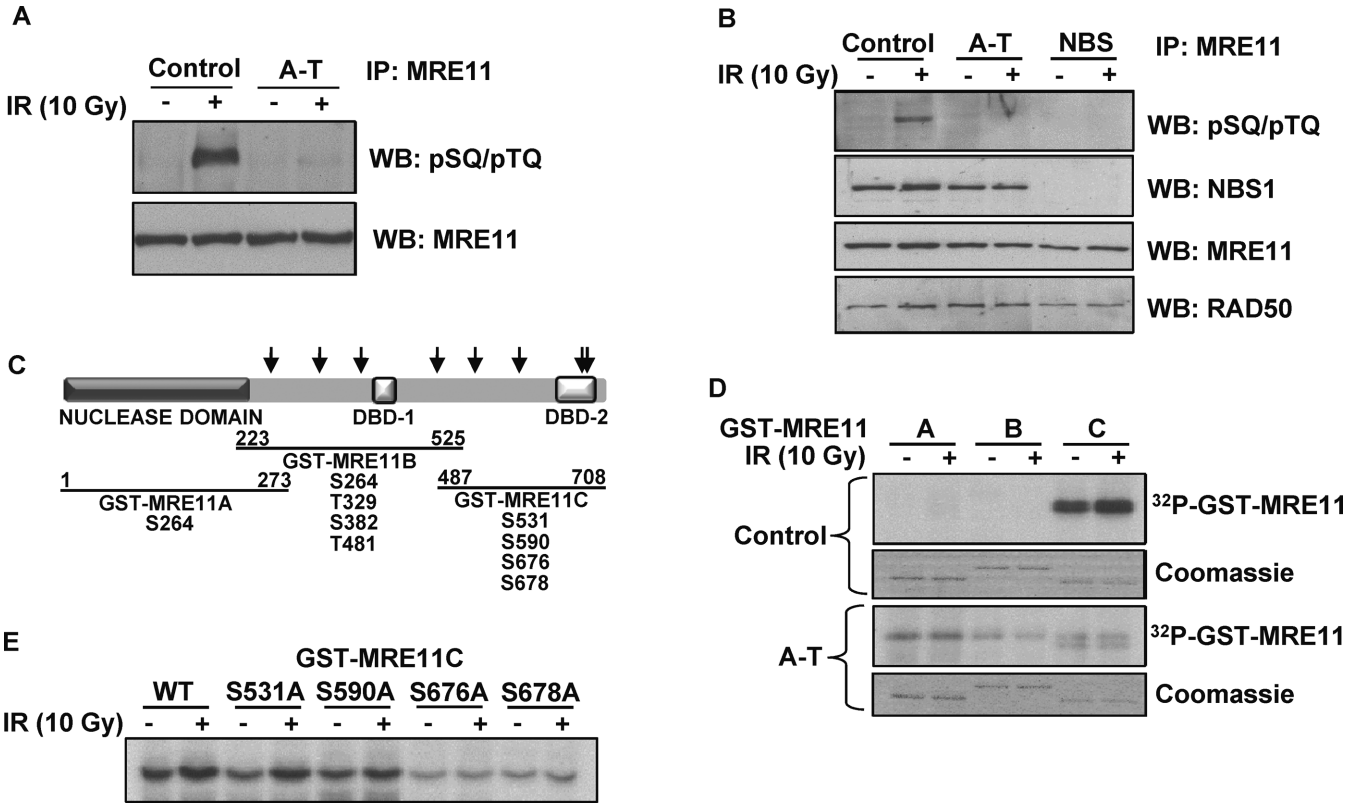

Figure 1. ATM-dependent phosphorylation of MRE11, its dependence on the MRN complex and identification of specific sites using *invitro* kinase assays. (**A**) Detection of MRE11 phosphorylation in cells treated with 10 Gy (+) or mock treated (−) by western blotting (WB) with a pSQ/pTQ antibody of immunoprecipitated (IP) MRE11 from both control and A-T cells. (**B**) Detection of MRE11 phosphorylation and MRN complex members in cells treated with 10 Gy IR (+) or mock treated (−) by western blotting (WB) with a pSQ/pTQ antibody and antibodies to the MRN complex members from control, A-T and NBS patient cells. (**C**) Schematic of putative ATM phosphorylation sites denoted by the target residues (↓), serine glutamine (SQ) or threonine glutamine(TQ) within the MRE11 protein with the three characterized domains of MRE11 shown, the nuclease domain and the two DNA binding domains (DBD) 1 and 2. The three overlapping GST tagged MRE11 fragments are shown. GST-MRE11A: 1-273aa; GST-MRE11B: 223-525aa; GST-MRE11C: 487-708aa and the SQ and TQ sites they each contain are specified. (**D**) ATM phosphorylates GST-MRE11C containing four putative SQ sites. *Invitro* kinase assays of immunoprecipitated ATM incubated with MRE11 GST fragments A, B and C with 10 Gy IR (+) or without (−) in both control cells and A-T cells. Autoradiographs and Coomassie staining are shown for each of the GST's spanning MRE11 A–C. (**E**) Alanine mutation of S676 and S678 cause a loss of GST-MRE11C phosphorylation. GST-MRE11C, containing four putative ATM SQ phosphorylation sites, were each mutated to alanine and used in ATM kinase assays to identify specific sites of phosphorylation after 10 Gy (+) or mock treatment (−).

the I-*Sce*1 meganuclease expression plasmid (pCMV-I-SceI) (46). Transfection efficiencies were determined by co-transfection of pCDNA3.1 filler plasmid with plasmid for WT *EGFP* expression in the recombination vector backbone. Cells were harvested 2 days post-transfection and analysed by FACS (FACSCanto, Becton Dickinson). DSB repair efficiencies were calculated as the proportion of EGFP positive cells corrected for transfection efficiency (86–92%) from three independent transfections. Cell cycle profiles were generated in parallel by staining of 5×10^5 cells with 300 μg/ml propidium iodide (Sigma Aldrich, USA) solution containing 0.1% Triton X-100 and 16 μg/ml of DNAse-free RNAse A. DNA content was determined using FACSCanto (Becton Dickinson) and data analysed by Modfit® software.

γH2AX kinetic

Cells were fixed with 4% paraformaldehyde unirradiated or 0.5, 3 or 8 h post 2 Gy irradiation. Immunostaining for γH2AX (Millipore) was performed as described previously by Lim *et al.* (47). The mean and standard deviation was calculated from three independent experiments of at least 30 cells having a minimum of 5 nuclear foci.

RAD51 kinetic

Cells were fixed with 4% paraformaldehyde unirradiated or 3, 6 or 16 h post 5 Gy irradiation. Cells were blocked with 5% bovine serum albumin (BSA) in 0.5% Triton X-100 phosphate buffered saline (PBS) then probed with 1/200 rabbit anti RAD51 (Santa Cruz, USA) antibody followed by anti-rabbit Alexa 488 (Invitrogen) in 2% BSA, 0.1% Triton X-100, PBS containing Hoechst. All slides were mounted with ProLong® Gold (Invitrogen) before viewing on a DeltaVision fluorescence microscopy system (Applied Precision). The mean and standard deviation was calculated from three independent experiments of at least 40 cells with a minimum of 5 nuclear foci.

IdU resection kinetics and immunostaining

Cells growing on coverslips were incubated with 20 μM iododeoxyuridine (IdU) overnight to label the genome. Cells were rinsed then either mock treated or irradiated with 5 Gy. Cells were returned to the incubator with media containing 1 μg/ml aphidicolin. Cells recovered for 2, 4 or 8 h before rinsing in PBS and pre-extracting with 0.4% Triton X-100, then fixed with 4% paraformaldehyde. Cells were permeabilized for 20 min with 0.4% Triton X-100, then blocked for 30 min with 10% BSA in PBST (phosphate buffered saline, 0.02% Tween 20) just prior to immunostaining. Cells were incubated with 1/15 mouse anti BrdU (BD Biosciences) for 1.5 h, washed then incubated with anti-mouse Alexa 594 secondary antibody (Life Technologies). G2 cells were detected by incubating with rabbit anti CENPF (Santa Cruz Technologies) followed by anti-rabbit 488 secondary (Life Technologies), then cells were finally counterstained with DAPI and mounted in Vectashield (Vector Laboratories). Imaging was performed on the Zeiss Axioscope and quantitation done using ImageJ on 8-bit greyscale images, maxima set at 30 (48).

RPA and CENPF immunostaining

Cells grown on coverslips were either unirradiated as controls or 2 h post 5 Gy IR were rinsed in PBS then pre-extracted with 0.2% Triton X-100, then fixed with 4% paraformaldehyde. Cells were permeabilized for 20 min with 0.2% Triton X-100, then blocked for 30 min with 10% BSA in PBST (phosphate buffered saline, 0.02% Tween 20) just prior to immunostaining. Cells were incubated with 1/300 mouse anti RPA34 (GeneTex) for 2 h, washed then incubated with anti-mouse Alexa 594 secondary antibody (Life Technologies). G2 cells were detected by incubating with rabbit anti CENPF (Santa Cruz Technologies) followed by anti-rabbit Alexa 488 secondary (Life Technologies), then cells were finally counterstained with DAPI and mounted in Vectashield (Vector Laboratories). Imaging was performed on the Zeiss Axioscope and quantitation done using ImageJ software, find maxima (point selection) function to measure intensities (48).

Phospho Exonuclease 1 immunostaining

Cells were left unirradiated or fixed 30 min post 5 Gy irradiation, then immunostained according to Bolderson *et al.* (49). Imaged on the DeltaVision fluorescence microscope (Applied Precision). The mean and standard deviation was calculated from three independent experiments.

Exonuclease 1 knockdown

U2OS cells were transfected with esiRNA (Sigma) against Exonuclease 1 by NEON electroporation (Life Technologies) then seeded onto coverslips. Forty-eight hours post-electroporation cells were either unirradiated as controls or 2 h post 5 Gy irradiation cells were immunostained as above for replication protein A (RPA) and CENPF. The mean and standard deviation was calculated from three independent experiments.

RESULTS

Radiation-induced phosphorylation of MRE11 is ATM-dependent and requires an intact MRN complex

To investigate the phosphorylation of MRE11, we employed a phospho-specific antibody that recognizes ATM consensus sites serine, glutamine (SQ) or threonine, glutamine (TQ). When cells were exposed to IR followed by immunoprecipitation of MRE11 and blotted with an SQ/TQ phospho-specific antibody (pSQ/pTQ), a marked response was observed in irradiated control cells (Figure 1A). To confirm that the band detected by the phospho-specific antibody was phosphorylated, immunoprecipitates were exposed to λ phosphatase which led to a loss of signal, supporting phosphorylation of MRE11 (Supplementary Figure S1A). Exposure of A-T cells (lacking functional ATM) to the same radiation dose failed to elicit any response at a molecular size corresponding to MRE11, indicating a requirement for ATM for the phosphorylation of MRE11 (Figure 1A). To further confirm that this phosphorylation was ATM-dependent we transfected A-T cells with an inducible ATM cDNA construct (50). The results in Supplementary Figure S1B demonstrate that induction of full-length ATM cDNA in transfected A-T cells, followed by exposure to IR, restored the phosphorylation of MRE11. No response was evident in transfected non-induced A-T cells. ATM and MRE11 have been previously shown to interact within a larger genome surveillance protein complex along with BRCA1 (51). To investigate the MRE11–ATM interaction in the context of a kinase and its substrate responding to damage, we performed co-immunoprecipitation with anti-MRE11 antibody and found no alteration in response to IR, supporting a constitutive interaction (Supplementary Figure S1C), which was not evident in A-T cells. Since MRE11 functions as part of the MRN complex, we determined whether the induction of MRE11 phosphorylation influenced MRN complex formation and whether the MRN complex can affect MRE11 phosphorylation. Immunoprecipitation of the MRN complex in control cells showed that IR induced phosphorylation of MRE11 did not influence the association between the members of the complex (Figure 1B). In an A-T cell line where phosphorylation of MRE11 is defective, association of the MRN complex was also normal (Figure 1B). However in an NBS1 deficient line (NBS), where MRE11 and RAD50 still associate, no radiation induced phosphorylation of MRE11 was observed at 10 Gy which is well above the dose known to activate ATM in NBS cells (52) (Figure 1B). This indicates that the presence of NBS1 is required in the complex for ATM to phosphorylate MRE11 in response to DNA damage.

ATM phosphorylates MRE11 at two specific sites, S676 and S678

To determine whether ATM directly phosphorylates MRE11 we used three overlapping fragments of MRE11 (GST-MRE11A, B and C) fused to glutathione S-transferase (GST) as substrates in an ATM-protein kinase assay (Figure 1C). Immunoprecipitated ATM phosphorylated GST-MRE11C (amino acids 487–708) from control cell lines and the activity increased after irradiation

(Figure 1D). Immunoprecipitates obtained from ATM deficient A-T cell lines showed no phosphorylation of this fragment (Figure 1D). GST-MRE11A (amino acids 1–273) and GST-MRE11B (amino acids 223–525) were not phosphorylated by ATM (Figure 1D). The four potential SQ phosphorylation sites in GST-MRE11C were altered by site-directed mutagenesis by introducing a serine to alanine mutation. Neither S531A nor S590A had any effect on the radiation-induced phosphorylation of MRE11 (Figure 1E). However when the S676 and S678 sites were mutated there was no evidence of radiation-induced phosphorylation suggesting that these two sites are phosphorylated on MRE11 by ATM (Figure 1E).

To confirm that MRE11 was being phosphorylated in cells after DNA damage a phospho-specific antibody to MRE11pS676pS678 (pSpS) was generated to investigate radiation-induced phosphorylation of this protein. The rabbit serum generated against the phosphorylated peptide (SKIM(pS)Q(pS)QVSC) was first depleted with antibodies binding to resin crosslinked to the non-phosphorylated form of the peptide and purified for subsequent use as an MRE11 antibody (nonP). While the phosphospecific antibody (pSpS) did not detect phosphorylated MRE11 by immunoblotting it was effective in immunoprecipitating phosphorylated MRE11 followed by detection with an anti-MRE11 antibody (GeneTex). The results in Figure 2A compare immunoprecipitations with anti-MRE11 (nonP) and MRE11 phospho-specific (pSpS) antibodies followed by immunoblotting with MRE11 antibody (GeneTex). A major band corresponding in size to MRE11 was only detected after irradiation in the pSpS immunoprecipitates (Figure 2A). In nonP anti-MRE11 antibody immunoprecipitates a prominent band was detected both in unirradiated and irradiated samples as expected. In both cases after irradiation a minor gel-shifted band was also detected (Figure 2A) which indicates that there are additional post-translational modifications to MRE11 taking place that had previously been reported using Xenopus extracts (40). As expected in ATLD2 cells which contain a truncated unstable MRE11 there was no detectable MRE11 when either antibody was used (Figure 2A).

Phosphorylation of MRE11 at these sites was shown to be dose dependent (Figure 2B). No signal was detected after irradiation in ATLD2 cells and a very much reduced response was seen in A-T cells. The phosphorylated form of MRE11 maintained its interactions with RAD50 and NBS1 as confirmed by co-immunoprecipitation (Figure 2B). This MRE11 phosphorylation increased with time in response to IR between 2–4 h post 5 Gy and subsequently decreased by 10 h (Figure 2C). Again no signal was observed in ATLD cells. We also showed that other agents capable of causing DNA DSB can induce this phosphorylation in addition to IR, including camptothecin and etoposide (Figure 2D). While the slower migrating band was detectable in all three cases it was most prominent after treatment with etoposide. A weaker signal was observed with H_2O_2 which causes primarily single strand DNA breaks and no phosphorylation in response to agents causing DNA crosslinks (cisplatin) or DNA alkylation (methyl methanesulfonate) was observed (Figure 2D).

Functional importance of ATM-dependent signalling through MRE11

To examine the cellular consequences of MRE11 phosphorylation we generated ATLD2hT cell lines complemented with WT MRE11 cDNA or a phosphosite mutant form of MRE11S676AS678A (MUT), which ablates the ATM-specific phosphorylation sites identified in this study. MRN complex formation was restored in ATLD2hT cells complemented with either WT or mutant (MUT) forms of MRE11 (Figure 3A). Immunoprecipitation of MRE11 in the vector only (VEC) cell line showed no significant amount of protein for any of the MRN complex members (Figure 3A). MRE11 is known to play a key role in ATM activation by autophosphorylation and subsequent downstream signalling to ATM substrates (22,53). We initially determined whether the MRE11 complemented ATLD cell lines could activate ATM normally. The results in Figure 3B show that the phosphosite MRE11 mutant (MUT) was still functioning in its role to activate ATM, displaying comparable levels of ATM autophosphorylation on S1981 as the WT in response to IR and as expected the vector cell line (VEC) showed very low levels of ATM-dependent phosphorylation on MRE11. ATM's activation after IR was confirmed by its subsequent signalling activity, phosphorylating several substrates including, KAP1 and SMC1 in response to DNA DSB (Figure 3B). The MUT cell line as expected showed comparative levels of phosphorylation of these substrates as was observed with the WT (Figure 3B). We next investigated the potential role of radiation-induced phosphorylation of MRE11 at these sites on cell survival. Our results showed that the vector only expressing cell line (VEC) displayed intermediate survival between control and A-T cells with increasing dose of IR (Figure 3C) as has been reported previously for ATLD cells (15). The WT expressing cell line (WT) corrected this sensitivity and produced a pattern of survival the same as the control cell line (NFF). The non-phosphorylatable mutant cell line (MUT) displayed intermediate levels of sensitivity, comparable to cells lacking functional MRE11 (VEC) revealing that specific phosphorylation of MRE11 played a key role in cell survival (Figure 3C). When we investigated the cell survival after IR for MRE11 cell lines mutated at either of the individual sites, S676A or S678A the same intermediate level of sensitivity was also observed as for the double mutant (S676AS678A). Increased chromosomal aberrations are observed in response to defective repair of DNA DSB and are an indicator of decreased cell survival. Previous data have shown that IR-induced chromosomal aberrations per metaphase are higher in A-T cells than in controls (54). The results in Figure 3D show that the vector cell line (VEC) was intermediate between control (NFF) and A-T cells as expected for ATLD and the MRE11S676AS678A mutant cell line (MUT) was approximately the same demonstrating a failure to correct these aberrations. This same intermediate level of aberrations was also observed for MRE11 cell lines mutated at either of the individual sites, S676A or S678A (Figure 3D). However, the WT MRE11 cell line showed a reduction of these aberrations to a level comparable to that in control cells (NFF) (Figure 3D). Together these results indicate that phosphorylation of MRE11 by

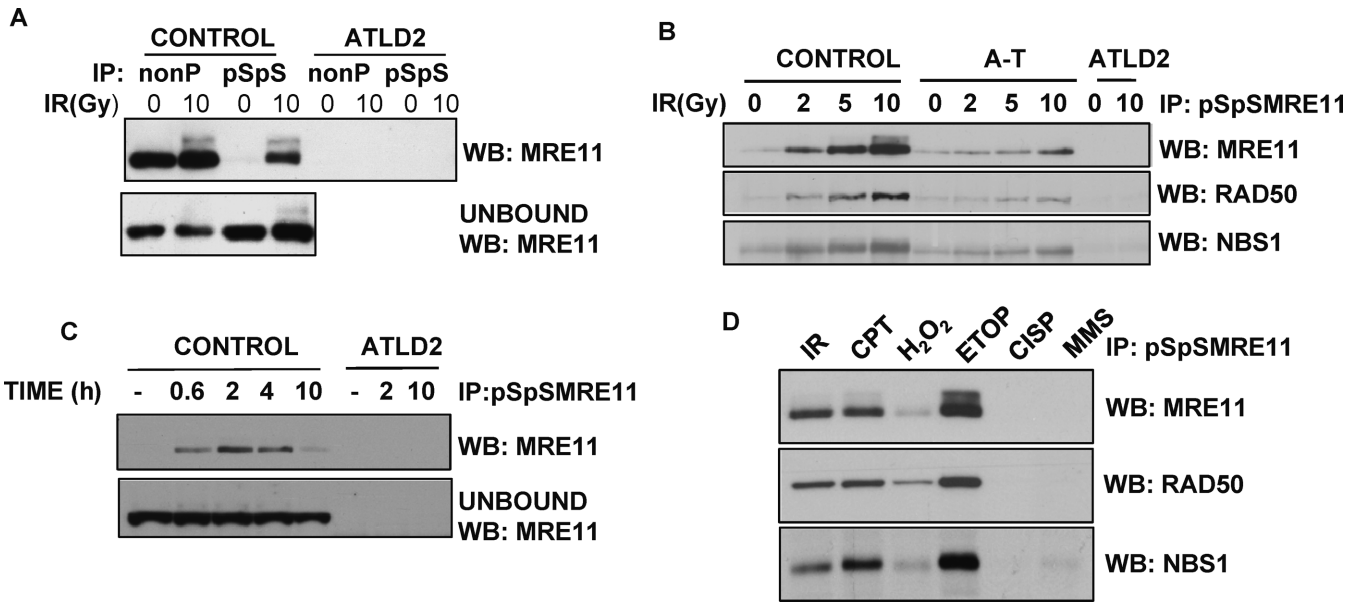

Figure 2. Investigation of MRE11 phosphorylation kinetics at MRE11S676S678. (**A**) MRE11pS676pS678 antibody immunoprecipitate the phosphorylated form of MRE11 after ionizing radiation (IR). Western blot (MRE11) of immunoprecipitated MRE11 using an antibody against MRE11S676S678 (nonP) site and the corresponding phosphorylated MRE11pS676pS678 (pSpS) sites from control and ATLD2 lymphoblastoid cells treated with 0 or 10 Gy IR. Unbound sample from each immunoprecipitation was run in parallel and also immunoblotted for total MRE11 (GeneTex). (**B**) Dose-dependent increase of MRE11 phosphorylation following IR. Western blot of immunoprecipitated MRE11 using an antibody against MRE11pS676pS678 (pSpSMRE11) sites from control and A-T lymphoblastoid cells treated with 0, 2, 5 or 10 Gy IR. ATLD2 cells were also run as a negative control (0 and 10 Gy). Western blot for the MRN complex proteins, MRE11, RAD50 and NBS1. (**C**) Increasing MRE11 phosphorylation over 2 h post 5 Gy. Western blot of immunoprecipitated MRE11 using an antibody against MRE11pS676pS678 (pSpSMRE11) sites from control lymphoblastoid cells either untreated (−) or harvested at 0.6, 2, 4 or 10 h post 5 Gy IR. ATLD2 lymphoblastoid cells were either untreated (−) or harvested at 2 and 10 h post 5 Gy IR and run as a negative control. (**D**) MRE11 phosphorylation in response to DNA double strand break inducing agents. Western blot of immunoprecipitated MRE11 using an antibody against MRE11pS676pS678 (pSpSMRE11) sites from control cells treated with either IR, camptothecin (CPT), hydrogen peroxide (H2O2), etoposide (ETOP), cisplatin (CISP) or methlymethanesulfonate (MMS).

ATM is required for cell survival through effective repair of DNA damage, and that both S676 and S678 sites of phosphorylation are also individually functionally important.

Phosphorylated MRE11 is recruited to sites of damage where it controls extent of resection

Recruitment of MRE11 to sites of damage is an early event required for repair of DNA damage. Using yellow fluorescent protein (YFP) tagged versions of MRE11 WT, mutant MRE11S676AS678A (MUT) or MRE11S676DS678D phosphomimetic (DD) to monitor this we found that all three were recruited to sites of DNA damage created by heavy ions (carbon ion) by co-localization of YFP-MRE11 with γH2AX (Figure 4A). To determine whether phosphorylation status of MRE11 might influence the rate of association with sites of damage, a live kinetic study was carried out which revealed a comparable rapid localization for all three forms of MRE11 (Figure 4B). In addition there was no visible effect on the dissociation of the phosphomimetic (DD) or alanine mutant (MUT) forms compared to the WT over the 12 h after damage (Figure 4C). It has previously been observed using *Xenopus* cell extracts that phosphorylation of MRE11 on S676 reduced its binding to DNA (40,55). Accordingly we investigated recruitment of the individual mutants (S676A and S678A) using heavy ion damage (uranium) (Figure 4D). Although there was no significant difference in the initial recruitment, a significant decrease in the localization was observed for the S678A mutant, where phosphorylation of S676 is still possible, indicating reduced stability in binding. There was no visible effect on the dissociation of either of the single alanine mutant forms compared to the WT over 12 h after damage (Supplementary Figure S2).

As there was no defect in the localization of the mutant MRE11S676AS67A to damaged chromatin, but these cells displayed an increase in chromosomal aberrations and decrease in survival after induction of DNA DSB, we performed a kinetic of γH2AX foci appearance and loss with time as a measure of break repair. In WT MRE11 corrected cells ∼80% of breaks were repaired by 8 h after IR whereas in both the VEC and MUT cell lines repair kinetics were slower with ∼50% of breaks still remaining after 8 h (Figure 4E). To investigate the apparent repair defect in the mutant cell line we employed GFP-based DNA repair reporter substrates to assess the performance of the MRE11S676AS678A mutant cell line in completing repair on various homology directed repair substrates previously characterized by Akyuz *et al.* (46). We observed a defect in microhomology-mediated NHEJ (mNHEJ) in both the MRE11S676AS678A (MUT) and vector (VEC) cell lines compared to the WT (Figure 5A). As expected (56), the VEC cell line was also defective in SSA and HR, but interestingly the MUT cell line showed comparable levels of SSA as WT but was defective in HR repair (Figure 5A). Since homology directed repair is a cell cycle phase-dependent

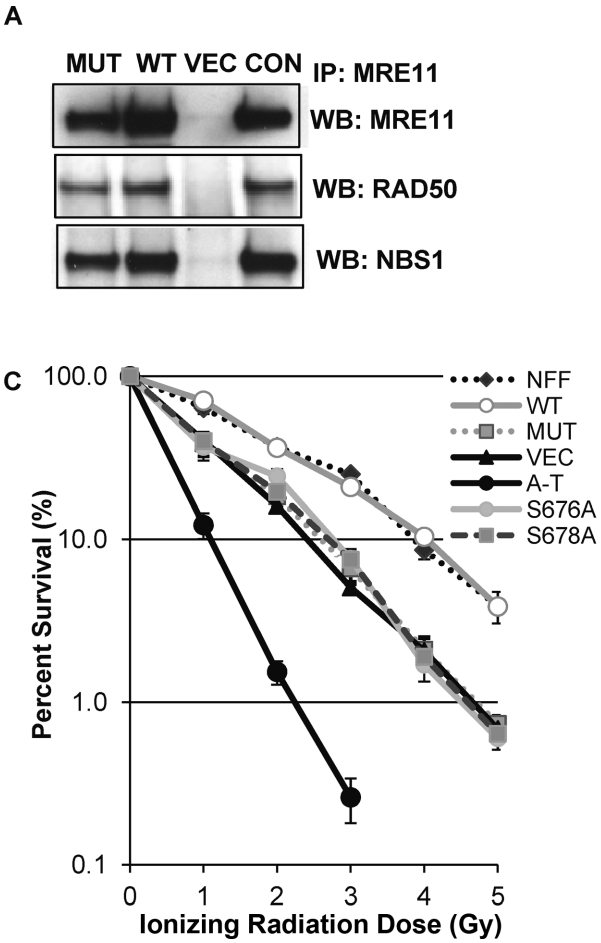

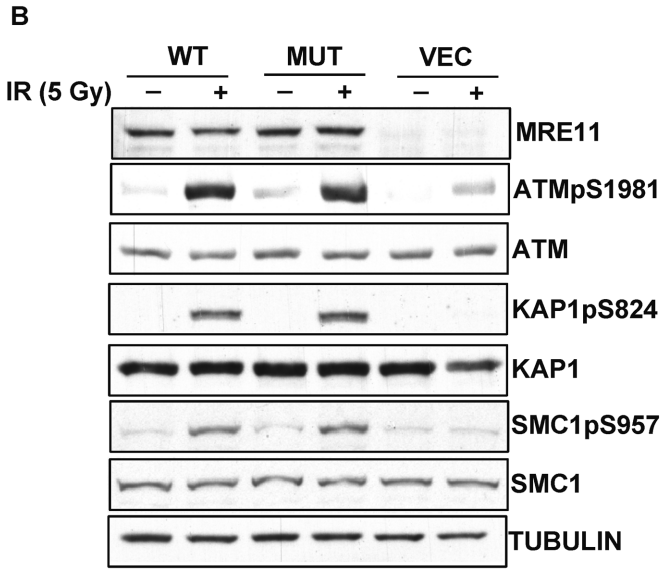

D

Cell line	Chromatid breaks	Chromosome breaks	Interchanges	ICA per Metaphase
NFF (50)	44	0	0	0.88
A-T (50)	166	7	0	3.46
WT (50)	41	2	0	2.69
MUT (27)	46	0	0	0.92
VEC (16)	66	1	0	2.48
S676A (20)	42	3	0	2.25
S678A (20)	39	1	1	2.05

Figure 3. Investigation of ATM signalling, cell survival and chromosomal aberrations in the cell line expressing non-phosphorylatable MRE11S676AS678A. (**A**) Stable MRN complex in WT and non-phosphorylatable mutant MRE11 corrected cell lines. Western blot of immunoprecipitated MRE11 from control (MCR5) and ATLDMRE11 (WT), ATLDS676AS678A (MUT) and ATLDVEC (VEC) cell lines. Also immunoblotted for NBS1 and RAD50. (**B**) ATM signalling in the non-phosphorylatable mutant MRE11 cell line is comparable to the WT corrected cell line. Total cell extracts from ATLDMRE11 (WT), ATLDS676AS678A (MUT) and ATLDVEC (VEC) cell lines were extracted 30 min post 5 Gy (+) or left as unirradiated controls (−) and western blotted for ATM S1981 autophosphorylation and total ATM, as well as the ATM kinase substrates, SMC1 and KAP1. Tubulin was immunoblotted as loading control. (**C**) The non-phosphorylatable mutant MRE11 cell line displays increased cellular sensitivity to IR. Plot of percent survival after 0, 1, 2, 3, 4 and 5 Gy IR. NFF (control), ATLDMRE11 (WT), ATLDS676AS678A (MUT), ATLDVEC (VEC), A-T, ATLDS676A (S676A) and ATLDS678A (S678A) cell lines were treated with increasing doses of IR and percent survival assessed by clonogenic cell survival assay. The mean ± standard deviation is plotted from 3 independent experiments. (**D**) Non-phosphorylatable mutant MRE11 cell line is unable to correct radiation induced chromosomal aberrations. Aberrations (chromatid breaks, chromosome breaks and interchanges) were scored from Giemsa stained metaphases in 2 Gy irradiated NFF (control), A-T, ATLDMRE11 (WT), ATLDS676AS678A (MUT), ATLDVEC (VEC), ATLDS676A (S676A) and ATLDS678A (S678A) cell lines. Induced chromosomal aberrations (ICA) were totalled and divided by number of metaphases as indicated in parentheses.

process we confirmed that the cell lines displayed comparable proportions of cells at each of the phases of the cell cycle (Supplementary Figure S3). Quantitation of this (Supplementary Figure S3B), showed that the WT (G2 = 17%) cell line displayed a slightly lower proportion of G2 cells as compared to MUT (G2 = 21%) and the vector (G2 = 22%) cell lines. To more specifically investigate DNA damage processed by the HR repair pathway, the kinetics of RAD51 recruitment, which promotes invasion of resected single stranded DNA was investigated. The vector (VEC) cell line showed impaired recruitment of RAD51 while recruitment was delayed in the MRE11S676AS678A mutant cell line (Figure 5B). More strikingly in both cases there was no significant loss of RAD51 foci over 16 h while foci were reduced to <50% in WT in that period. These data indicate a delayed or impaired resolution of these HR substrates which was compatible with reduced HR observed using the GFP reporter substrate assay (Figure 5A).

MRE11 has been shown to play a catalytic role during homology directed repair where it nicks the DNA upstream from the break then resects in a 3′→5′ direction towards the break with more extensive resection being performed primarily by the 5′→3′ Exonuclease 1 (8–12). As resection is the first step in the repair of all homology directed repair pathways we determined the kinetics of resection in response to IR by pre-labeling cells with a thymidine analog, iododeoxyuridine (IdU), followed by quantitating the foci of resected single stranded DNA labelled with IdU in G2 phase cells (57). In normal control (NFF) and MRE11 WT corrected cells a peak of induction occurred at 2 h fol-

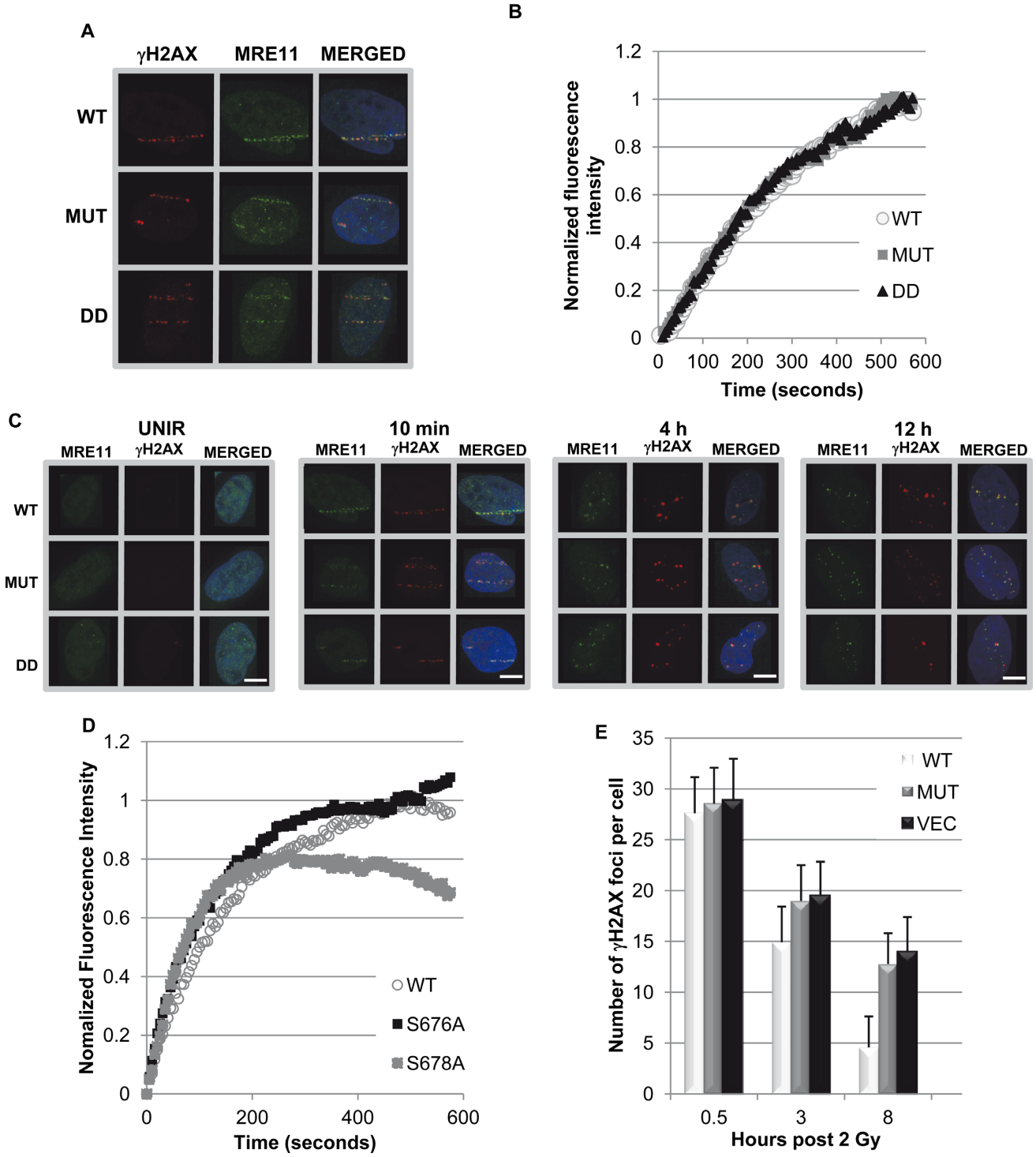

Figure 4. Phosphorylation status does not affect recruitment of YFP tagged MRE11 to sites of breaks or its loss from these sites but DNA repair is defective. (**A**) YFP tagged MRE11 (green) co-localized with γH2AX (red) to carbon ion tracks of damage in U2OS cells. YFP-MRE11 (WT), YFP-MRE11S676AS678A (MUT) or phosphomimetic YFP-MRE11S676DS678D (DD) were transfected into U2OS cells, fixed 10 min post damage and counterstained with DAPI (blue). (**B**) Real time quantitation of YFP tagged MRE11 localizing to sites of damage. YFP-MRE11 (WT), YFPMRE11S676AS678A (MUT) or phosphomimetic YFP-MRE11S676DS678D (DD) in U2OS cells being recruited to sites of carbon ion damage during the first 10 min post damage. (**C**) Dissociation of YFP tagged MRE11 (green) from carbon ion tracks of damage in U2OS cells. YFP-MRE11 (WT), YFP-MRE11S676AS678A (MUT) or phosphomimetic YFP-MRE11S676DS678D (DD) were transfected into U2OS and samples fixed as unirradiated (UNIR), 10 min, 4 or 12 h post damage then immunostained with γH2AX (red) and counterstained with DAPI (blue). The bar represents 10 μm. (**D**) Real time quantitation of YFP tagged MRE11 localizing to sites of damage. YFP-MRE11 (WT), YFPMRE11S676A (S676A) or YFP-MRE11S678A (S678A) in U2OS cells being recruited to sites of uranium ion damage during the first 10 min post damage. (**E**) Reduced repair efficiency of DSBs in the non-phosphorylatable mutant and vector cell lines. The formation and repair of DSBs marked by γH2AX immunostaining in response to 2 Gy IR. Foci were counted from three independent experiments and the mean and standard deviation plotted.

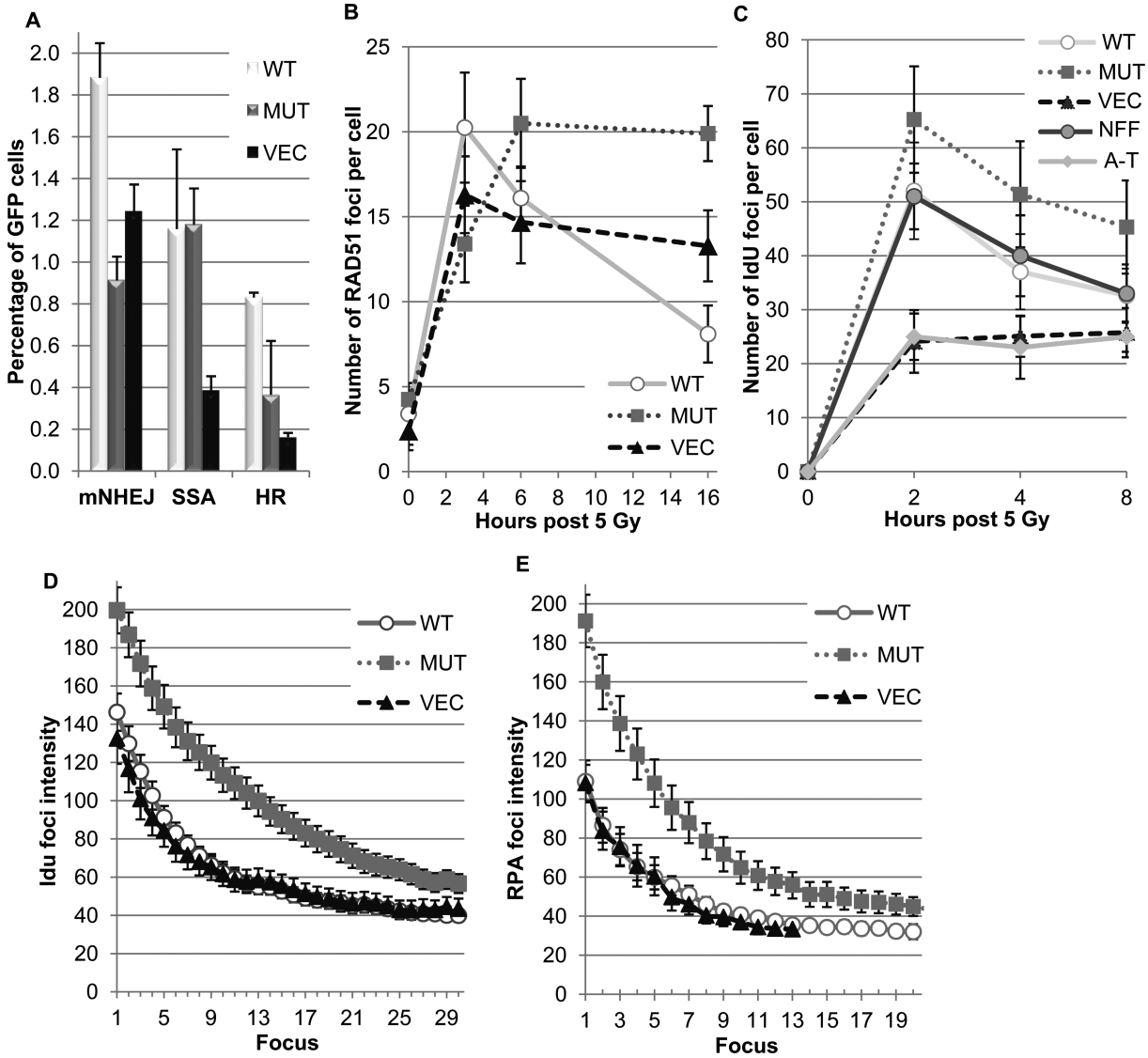

Figure 5. The non-phosphorylatable mutant (MRE11S676AS678A) cell line is defective in homology directed repair and a greater extent of resection (single stranded DNA) is observed in these cells. (**A**) Assaying for DSB repair function using GFP reporter substrates. GFP reporter substrates for microhomology-mediated non-homologous end joining (mNHEJ), single strand annealing (SSA) and homologous recombination (HR) were co-transfected with the meganuclease, I-Sce1 expression plasmid. Percentage of GFP positive cells, indicating successful repair, was plotted for each cell line ATLDMRE11 (WT), ATLDS676AS678A (MUT) and ATLDVEC (VEC). These data were corrected for transfection efficiency (86-92%). I-Sce1 negative controls (GFP reporter substrate and filler plasmid) transfections were always 0-0.1%. The mean and standard deviation is plotted from three transfections. (**B**) Defects in RAD51 filament formation during HR. Quantitation of RAD51 foci in unirradiated and 3, 6 and 16 h post 5 Gy irradiation of ATLDMRE11 (WT), ATLDS676AS678A (MUT) and ATLDVEC (VEC) cell lines. The mean and standard deviation is plotted from three independent experiments. (**C**) Kinetics of resection during homology directed repair. Quantitation of the number of foci of resected single stranded DNA labelled with iododeoxyuridine (IdU) in G2 cells at 2, 4 and 8 h, post 5 Gy irradiation of the cell lines ATLDMRE11 (WT), ATLDS676AS678A (MUT) and ATLDVEC (VEC). The mean and standard deviation is plotted from three independent experiments. (**D**) Extent of resection measured by IdU focus intensity in G2 cells 2 h post 5 Gy. The intensity of each IdU focus for a total of 60–90 cells for each cell line, ATLDMRE11 (WT), ATLDS676AS678A (MUT) and ATLDVEC (VEC) was estimated using ImageJ find maxima (point selection) function. The mean intensity of the 30 most intense foci for each cell was plotted with 95% confidence intervals from two independent experiments. The three most intense foci for each cell line was removed due to saturation which would prevent quantitative comparisons. (**E**) Extent of resection measured by RPA focus intensity in G2 cells 2 h post 5 Gy. The intensity of each RPA focus for a total of 60–90 cells for each cell line, ATLDMRE11 (WT), ATLDS676AS678A (MUT) and ATLDVEC (VEC) was estimated using ImageJ maxima (point selection) function. The mean intensity of the 20 most intense foci for each cell was plotted with 95% confidence intervals from two independent experiments. The two most intense foci for each cell line was removed due to saturation which would impair quantitative comparisons.

lowed by a gradual loss of single stranded regions over the subsequent 6 h (Figure 5C). A similar pattern was observed in MRE11S676AS678A cell line (MUT), but the curve was shifted upwards, although not significantly different to control. The vector cell line (VEC) showed a reduced number of sites of resection and there was no significant loss of these sites up to 8 h post-irradiation. The apparent increase in IdU foci in the MRE11 mutant could be due to an increase in the number of sites of damage or due to increased intensity of labelling at individual sites indicative of more extensive resection. We investigated this further by quantitating IdU focus intensity in G2 phase cells, from a total of 60–90 cells for each cell line (Figure 5D). It is evident that the mutant cell line exhibits greater focus intensity than the WT across the range of foci investigated suggesting greater levels of resection at all sites of repair. The coincidence of the vector only and WT curves shows that the extent of resection is similar in both although less sites are involved in the vector only cell line compared to the WT as is evident from Figure 5C. We also used RPA as a marker of resection in G2 phase cells and obtained data comparable to those with IdU, again supporting more extensive resection in the MRE11 mutant (Figure 5E). Thus MRE11 phosphorylation appears to be required to control the extent of resection at any given site undergoing homology directed repair.

Control of extent of resection by MRE11 phosphorylatin is through Exonuclease1

Previous data from yeast suggested that phosphorylation of Exonuclease 1 is involved in a negative feedback loop to limit accumulation of single strand DNA during resection and DNA damage checkpoint activation (58). There is also evidence that phosphorylation of this protein by ATM is required for recruitment of DNA repair proteins and regulation of HR (49). To determine whether the phosphorylation status of Exonuclease 1 was playing a role in the extensive resection observed in the non-phosphorylatable MRE11S676AS678A mutant cell line (MUT), we performed immunostaining with an antibody against Exonuclease 1 pS714 (EXO1pS714) to demonstrate co-localization of the phosphorylated form with γH2AX in irradiated control (NFF) cells (Figure 6A). Since phosphorylation at this site has been shown to be ATM-dependent it was not surprising that Exonuclease 1 phosphorylation was only observed at a low level in vector cell line (VEC) which was supported by quantitation (Figure 6B). The Exonuclease1 pS714 foci in the WT MRE11 cell line co-localized with γH2AX (Figure 6A) and quantitation of these foci revealed levels similar to those in NFF control cells (Figure 6B). On the other hand, the phosphorylation foci in the MRE11S676AS678A mutant cell line (MUT) were markedly reduced and quantitation of these showed low levels that were comparable to those in an A-T cell line (Figure 6B). To confirm these data we also carried out immunoblotting with an anti-Exonuclease 1 pS714 antibody. The results in Figure 6C show that Exonuclease 1 is phosphorylated in WT MRE11 cells but neither the MUT nor VEC cell lines showed evidence of phosphorylation of Exonuclease 1. To determine the dependency of resection on Exonuclease 1 in each of these cell lines, WT MRE11, MRE11S676AS678A (MUT) and vector (VEC), Exonuclease 1 was knocked down (Figure 6D). We observed a comparable reduction in the proportion of G2 phase cells with RPA foci in all three cell lines after Exonuclease 1 knockdown (Figure 6E), supporting a significant role for Exonuclease 1 in each of these cell lines displaying ∼30% reduction. As might be expected there was a reduced level of G2 cells undergoing resection in the vector cell line (VEC) where there is no functional MRE11. To further investigate this role for Exonuclease 1 in the overextended resection phenotype, we employed previously characterized GFP tagged Exonuclease 1 non-phosphorylatable (EXO1S714A) and phosphomimetic (EXO1S714E) mutants (49). We investigated RPA foci intensity as a measure of extent of resection in U2OS cells where we obtained transfection efficiency of 66% (SD = 3) at 24 h (Supplementary Figure S4A). A similar extent of overexpression was observed for WT GFP-Exonuclease 1, EXO1S714A (SA) and EXO1S714E (SE) mutants as determined by western blot analysis (Supplementary Figure S4B). GFP-EXO1 signal was lost during the pre-extraction conditions used to immunostain RPA foci (resection) so the foci intensities were determined from a mix of transfected and untransfected G2 phase cells. The G2 phase U2OS cells transfected with the non-phosphorylatable EXO1S714A mutant showed a small increase in the average RPA foci intensity as compared to WT from the most intense to least intense focus (Supplementary Figure S4C). On the other hand the EXO1S714E phosphomimetic mutant transfected U2OS cells showed on average less intense foci in G2 cells as compared to the WT (Supplementary Figure S4C).

Together the data presented suggest that phosphorylation of MRE11 plays a key role in determining extent of resection and that in the absence of this phosphorylation there is inefficient ATM-dependent phosphorylation of Exonuclease 1 which contributes to uncontrolled resection at any particular DSB site undergoing homology directed repair.

DISCUSSION

The novel findings described here demonstrate the importance of ATM-dependent phosphorylation of MRE11 at two specific sites, S676 and S678 after DSB inducing agents. Phosphorylation at these sites is critical for repair of DSB and cell survival. This ATM-dependent phosphorylation of MRE11 is not, however, required for the formation of the MRN complex, the activation of ATM kinase or its localization to sites of DNA damage. This is consistent with previous cytological analysis of the MRN complex showing that its association with chromatin or damaged DNA does not depend on ATM (18,59). MRE11 represents the third member of the complex to be phosphorylated by ATM in response to DNA damage. ATM-dependent phosphorylation of NBS1 occurs on two sites, S282 and S343 (26,30) and mutation at these sites prevents signalling to downstream substrates linked to DNA repair, cell cycle checkpoint activation and cell survival (30,31,60). A single site of ATM-dependent phosphorylation (S635) has been identified on the second member of the complex, RAD50 (27). Phosphorylation at this site is required for correction of cell cycle checkpoint activation, DNA repair and survival

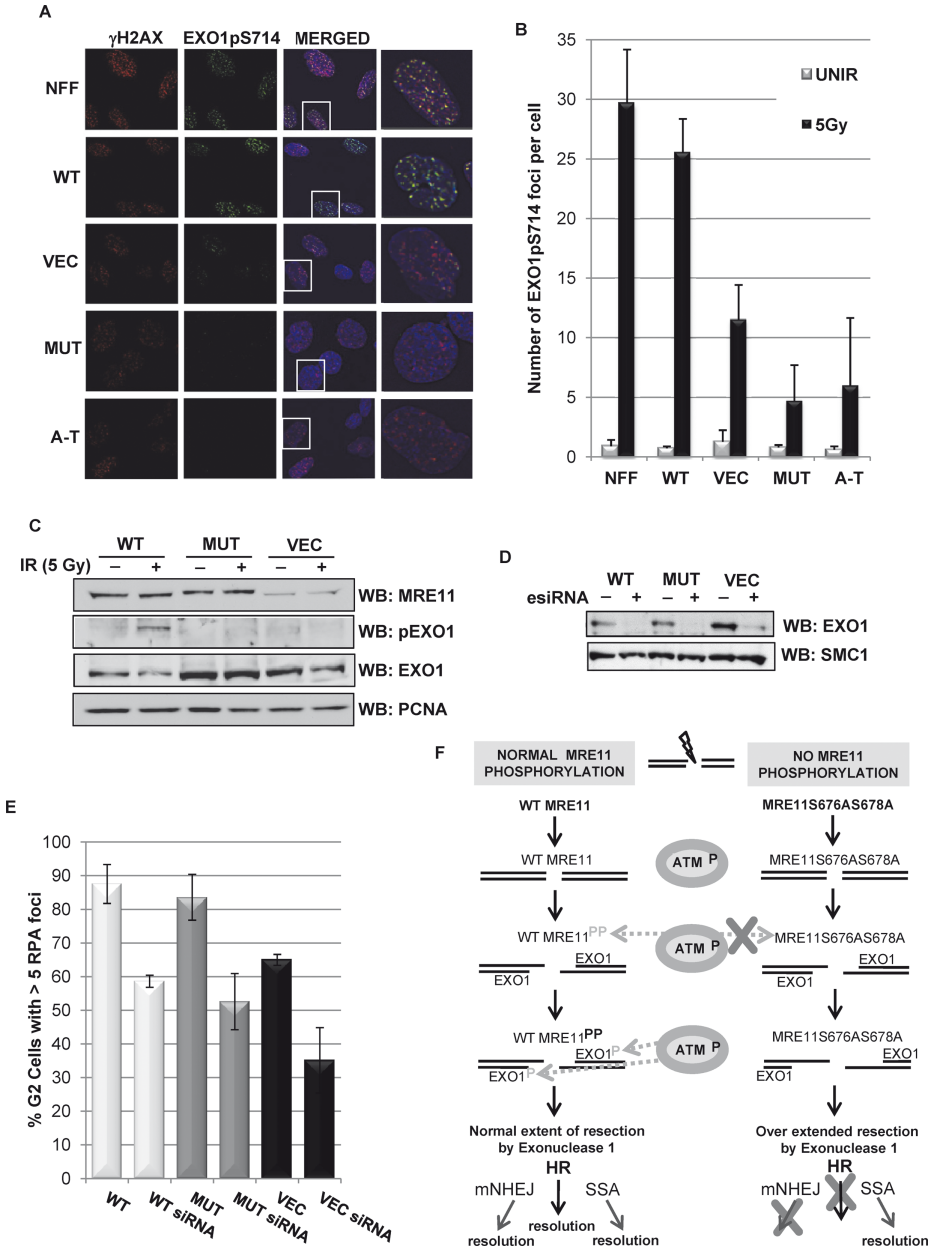

Figure 6. Defect in ATM phosphorylation of Exonuclease 1 in the MRE11S676AS678A mutant cell line. (**A**) Immunostaining of γH2AX (red) and EXO1pS714 foci (green) in response to 5 Gy IR for each cell line ATLDMRE11 (WT), ATLDS676AS678A (MUT) and ATLDVEC (VEC) as well as NFF (control) and A-T cell lines after 30 min. The merged image including DAPI staining is shown and the boxed cell has been enlarged in the far right panel. (**B**) Quantitation of Exonuclease 1 (EXO1pS714) foci in unirradiated (UNIR) and 5 Gy irradiated cells for each cell line ATLDMRE11 (WT), ATLDS676AS678A (MUT) and ATLDVEC (VEC) as well at NFF (control) and A-T cell lines after 30 min. The mean and standard deviation of three independent experiments is plotted. (**C**) Western blot of total cell extracts from ATLDMRE11 (WT), ATLDS676AS678A (MUT) and ATLDVEC (VEC) cell lines for phosphorylated (S714) Exonuclease 1 (pEXO1) and total Exonuclease 1 (EXO1) from unirradiated (−) and 5 Gy irradiated cells (+). PCNA is shown as loading control. (**D**) Western blot of total cell extracts from ATLDMRE11 (WT), ATLDS676AS678A (MUT) and ATLDVEC (VEC) cell lines for Exonuclease 1 (EXO1) with (+) and without (−) knockdown of Exonuclease1 by esiRNA (Sigma) after 48 h. SMC1 is shown as loading control. (**E**) Effect of Exonuclease 1 knockdown on the proportion of G2 phase cells with RPA foci for ATLDMRE11, ATLDS676AS678A and ATLDVEC cell lines. Cells were transfected with esiRNA (WT siRNA, MUT siRNA and VEC siRNA) or mock transfected (WT, MUT and VEC) for 24 h. Cells were irradiated with 5 Gy and immunostained with CENPF and RPA then G2 positive cells counted containing >5 foci after 2 h. The mean and standard deviation of three independent experiments is plotted. (**F**) Schematic model showing the role of MRE11 phosphorylation by ATM in response to DSB induction. The occurrence of DSB activates the DSB signalling cascade involving autophosphorylated ATM (ATMP) to initiate its repair. After the induction of resection ATMP phosphorylates MRE11 at S676 and S678 (WT MRE11PP) which acts as an adaptor for ATMP-dependent phosphorylation of Exonuclease 1 (EXO1P), controlling the extent of resection. This enables RAD51 to catalyze strand invasion and subsequent completion of HR repair or subsequent repair by the other pathways requiring end processing like microhomology-mediated non-homolgous recombination (mNHEJ) and SSA. If MRE11 is not phosphorylatable (MRE11S676AS678A) ATM is still normally autophosphorylated (ATMP) leading to induction of end processing, but in the absence of MRE11 phosphorylation there is no subsequent ATM-dependent phosphorylation of Exonuclease 1 (EXO1) leading to over extended resection by EXO1. Although RAD51 is recruited it largely fails to catalyze efficient strand invasion leading to a failure of the less error prone HR. But the SSA pathway is still functional as it can tolerate the extensively resected single stranded DNA unlike the other forms of homology directed repair.

in RAD50-deficient cells in response to DNA DSB (27). In contrast to the other two members of the complex, MRE11 is phosphorylated at two adjacent sites in the ATM substrate consensus sequence $S^{676}Q$ $S^{678}Q$. The corresponding MRE11 phosphosite mutant enables normal ATM signalling through substrates such as SMC1, the phosphorylation of which is implicated in cell cycle control, genome stability and cell survival (27,28,52,61). What stands out in the present study is ATM-mediated control of Exonuclease 1 activity limiting the extent of resection. Interestingly another kinase, Ribosomal S6 kinase (Rsk) has recently been suggested to also phosphorylate MRE11 at S676, although this site in MRE11 does not conform to its consensus sequence (55). They showed that when Rsk is overexpressed as has been found in some cancer cells it could phosphorylate MRE11 on S676 in response to treatment with neocarzinostatin leading to a much reduced activation of ATM (S1981 phosphorylation) inhibiting checkpoint activation. This may indicate an overlap or competition between ATM and Rsk under certain circumstances for this site on MRE11.

This investigation of the role of MRE11 phosphorylation in DNA repair provided evidence for an important quality control function in the major DNA DSB repair pathway, homology directed repair. Discrimination of the early role of MRE11 in DNA damage recognition and ATM activation, which were normal in the phosphosite mutant cell line, facilitated analysis of its later role in repair, providing a unique separation of function mutant MRE11. The early steps of homology directed repair require resection by MRE11 and other nucleases (8–10,12). The extent of this resection has been shown to be different for mNHEJ, SSA and HR, where mNHEJ and HR which share the initial end resection steps require limited resection as compared to SSA which may involve larger regions (11,62). Here we show that both mNHEJ and HR require MRE11 phosphorylation to control the extent of resection. Further downstream this appears to be controlled by ATM-mediated phosphorylation of Exonuclease 1 at S714 which limits its activity. Thus in the absence of MRE11 phosphorylation, DNA DSB sites that are processed for homology directed repair are over resected and cannot be processed properly by RAD51 for strand invasion and subsequent HR. However, as we have demonstrated these single stranded tails can still be processed by the SSA pathway which would be predicted to lead to large losses of genetic material (Figure 6D). The defect in HR and over reliance on SSA would explain the decreased survival and high rates of chromosomal aberrations, particularly chromatid type, in these cells. The mNHEJ pathway unlike the other two pathways mentioned above does not lead to RAD51 recruitment, it relies on minimal resection leading to microhomology annealing and repair. So in the absence of MRE11 phosphorylation the observed failure of mNHEJ repair pathway may simply be explained by the overextended resection of the reporter substrate which requires 23 bp of processing to restore GFP signal (Figure 5A) (46).

We did not observe any significant change in the MRE11S676AS678A mutant cell line with regard to the choice of repair pathway early in the repair process, as assessed by the number of sites of resection, but did observe downstream effects on final repair outcome due to the over resection occurring at sites, causing a bias away from the less error prone HR pathway. More recently, Tomimatsu *et al.* (63) found that Exonuclease 1 is also phosphorylated by CDKs at four sites regulating the pathway switch between HR and NHEJ in the repair of a DSB. Specifically they found that without CDK phosphorylation (the non-phosphorylatable alanine mutant of Exonuclease 1) they saw a reduction in the number of sites of resection and a subsequent decrease in HR based repair. In addition, the phosphomimetic mutant displayed an increase in the number of sites of resection and a decrease in subsequent NHEJ (63). These data suggest that phosphorylation of Exonuclease 1 by CDK, at sites distinct from those phosphorylated by ATM, determine the early pathway decision between HR and NHEJ, whereas phosphorylation of Exonuclease 1 by ATM determines the extent of resection.

Both MRE11 and Exonuclease 1 have been shown to be critical for the process of resection (9,10,12,49,64). Interestingly Exonuclease 1 is phosphorylated on S714 by ATM in response to DSB in a kinetic that correlates with the end of resection (49). The timing of this phosphorylation is important as a phosphomimetic Exonuclease 1 (EXO1S714E) curtails resection (decreased number of sites of resection as assessed by RPA foci). Bolderson *et al.* (49) also found that a non-phosphorylatable mutant or a phosphomimetic of Exonuclease 1 interfered with subsequent RAD51 recruitment and successful HR. These observations and the data presented here demonstrating Exonuclease1 phosphorylation status in the resection phenotype support our findings that phosphorylation of Exonuclease 1 is the signal to terminate resection to provide an optimal substrate for successful completion of HR.

The MRN complex is proposed to tether broken DNA ends until they are repaired (65,66). Previous studies by Virgilo *et al.* (40) and Chen *et al.* (55) have investigated affinity and phosphorylation status of MRE11 binding to DNA. Briefly Virgilio *et al.* (40) using *Xenopus* extracts incubated with DSB-containing DNA demonstrated hyperphosphorylation of MRE11 involving eight SQ/TQ ATM/ATR consensus sites, including $S^{676}Q$ and $S^{678}Q$, as well as sites phosphorylated by other kinases. Substitution of all eight of the S/T for A (MRN-SA) resulted in a significant increase in MRE11 binding to DNA or chromatin while the phosphomimetic mutant (MRN-SD) showed dramatically reduced binding and it was concluded that phosphorylation of MRE11 SQ/TQ motifs, facilitates the release of the complex from DNA and represents a signal for the control of DNA repair. Additionally the study of MRE11 phosphorylation by Chen *et al.* (55) also using *Xenopus* extracts showed that when MRE11 became phosphorylated by Rsk or Moloney sarcoma oncogene (Mos) kinase treatment at S676 it displayed decreased affinity to dsDNA-bound avidin beads. They went on to show increased retention of MRE11 foci in cells expressing MRE11S676A. Although S676 and S678 phosphorylation sites are within the second putative DNA binding domain of MRE11 we failed to observe any effect on MRE11 recruitment with the quantitative live kinetic or later retention/loss over time at sites of damage using either the alanine non-phosphorylatable MRE11 mutant or the aspartic acid phosphomimetic mu-

tant in human cells. The disparity of our observations to those previously published may be that the retention/loss of MRE11 over time (12 h) is not quantitative so we may not be detecting more subtle changes in localization at later time points. Although the MRE11S678A single mutant, where S676 could be phosphorylated, did show a destabilized binding compared to WT or MRE11S676A form as would be predicted based on the previously discussed studies (40,55).

While our observations do not provide evidence for dissociation of phosphorylated MRE11 from chromatin to terminate resection after ATM dependent phosphorylation on $S^{676}QS^{678}Q$ we have presented more mechanistic insight into the process showing that phosphorylation of MRE11 is required for phosphorylation of Exonuclease 1 controlling the extent of resection. In contrast to NBS1 and RAD50, we did not observe a defect in signalling through SMC1 but have instead identified Exonuclease 1 as a substrate critical in signalling to DNA repair. Morin *et al.* (58) have shown that Exonuclease 1 is inhibited by phosphorylation in yeast and that this phosphorylation has an important function in modulating the cellular response to DNA damage. Their data suggest that Exonuclease 1 phosphorylation downregulates its activity to limit the accumulation of ssDNA at damaged sites. This is consistent with our results where a phosphosite mutant of MRE11 was defective in controlling the extent of resection during repair of DNA DSB.

Our study largely focused on the two sites $S^{676}Q$ $S^{678}Q$ as the initial results on cell survival and chromosomal aberrations were comparable between the single and double site mutations, suggesting redundant roles. Whether this is due to their close proximity and thus mutation of an individual site is affecting the other or if there is potential coordination between these two sites in bringing about the observed cellular responses investigated here has been largely unexplored. Antibodies to the individual sites would help to explore the kinetics of phosphorylation of the sites individually and how this might influence repair. The characterization of the non-phosphorylatable (MRE11S676AS678A) mutant form of MRE11 has not only shed light on the key role of this phosphorylation in controlling the extent of resection enabling successful HR by controlling ATM's phosphorylation of Exonuclease 1 but also provides a separation of function mutation enabling a distinction between the early role of MRE11 in activating ATM from its more downstream roles in controlling resection during homology directed repair. Our observations clearly demonstrate that the ATM-dependent phosphorylation of MRE11 is critical for the DNA damage response as observed previously for phosphorylation of NBS1 (26,28–31) and RAD50 (27). While all three proteins perform an adaptor role for ATM-dependent downstream signalling it is also evident that the individual phosphorylations have different functional consequences. The results here further underpin the essential intertwined roles that ATM and the MRN complex play as caretakers of the genome.

SUPPLEMENTARY DATA

Supplementary Data are available at NAR Online.

ACKNOWLEDGEMENTS

We would like to thank Olivia Barton for providing methodological advice with IdU resection assay; Gudrun Becker for technical assistance with heavy ion experiments; Steve Jackson who provided the ATLD2hT cell line; Jean-Yves Masson for providing the pEYFP-MRE11 clone; Shaun P. Scott for initiating this project and performing some of the preliminary data with the pSQ/pTQ antibody and kinase assays; Philip Chen for performing the survival and chromosomal aberration experiments; Aine Farrell for maintenance of cell resources and the other members of the Lavin laboratory for helpful feedback over the many years. We acknowledge QIMR Berghofer where the ground work of this project was performed.

FUNDING

Queensland Cancer Council [ID1042912]; NHMRC [APP1020028]; BMBF [02NUK002A]. Funding for open access charge:
Conflict of interest statement. None declared.

REFERENCES

1. Ciccia,A. and Elledge,S.J. (2010) The DNA damage response: making it safe to play with knives. *Mol. Cell*, **40**, 179–204.
2. Wang,C. and Lees-Miller,S.P. (2013) Detection and repair of ionizing radiation-induced DNA double strand breaks: new developments in nonhomologous end joining. *Int. J. Radiat. Oncol. Biol. Phys.*, **86**, 440–449.
3. Zhou,Y. and Paull,T.T. (2013) DNA-dependent protein kinase regulates DNA end resection in concert with Mre11-Rad50-Nbs1 (MRN) and ataxia telangiectasia-mutated (ATM). *J. Biol. Chem.*, **288**, 37112–37125.
4. Richard,D.J., Cubeddu,L., Urquhart,A.J., Bain,A., Bolderson,E., Menon,D., White,M.F. and Khanna,K.K. (2011) hSSB1 interacts directly with the MRN complex stimulating its recruitment to DNA double-strand breaks and its endo-nuclease activity. *Nucleic Acids Res.*, **39**, 3643–3651.
5. Escribano-Diaz,C., Orthwein,A., Fradet-Turcotte,A., Xing,M., Young,J.T., Tkac,J., Cook,M.A., Rosebrock,A.P., Munro,M., Canny,M.D. *et al.* (2013) A cell cycle-dependent regulatory circuit composed of 53BP1-RIF1 and BRCA1-CtIP controls DNA repair pathway choice. *Mol. Cell*, **49**, 872–883.
6. Falck,J., Forment,J.V., Coates,J., Mistrik,M., Lukas,J., Bartek,J. and Jackson,S.P. (2012) CDK targeting of NBS1 promotes DNA-end resection, replication restart and homologous recombination. *EMBO Rep.*, **13**, 561–568.
7. Symington,L.S. and Gautier,J. (2011) Double-strand break end resection and repair pathway choice. *Annu. Rev. Genet.*, **45**, 247–271.
8. Nimonkar,A.V., Genschel,J., Kinoshita,E., Polaczek,P., Campbell,J.L., Wyman,C., Modrich,P. and Kowalczykowski,S.C. (2011) BLM-DNA2-RPA-MRN and EXO1-BLM-RPA-MRN constitute two DNA end resection machineries for human DNA break repair. *Genes Dev.*, **25**, 350–362.
9. Garcia,V., Phelps,S.E., Gray,S. and Neale,M.J. (2011) Bidirectional resection of DNA double-strand breaks by Mre11 and Exo1. *Nature*, **479**, 241–244.
10. Tomimatsu,N., Mukherjee,B., Deland,K., Kurimasa,A., Bolderson,E., Khanna,K.K. and Burma,S. (2012) Exo1 plays a major role in DNA end resection in humans and influences double-strand break repair and damage signaling decisions. *DNA Repair (Amst).*, **11**, 441–448.
11. Truong,L.N., Li,Y., Shi,L.Z., Hwang,P.Y., He,J., Wang,H., Razavian,N., Berns,M.W. and Wu,X. (2013) Microhomology-mediated End Joining and Homologous Recombination share the initial end resection step to repair DNA double-strand breaks in mammalian cells. *Proc. Natl. Acad. Sci. U.S.A.*, **110**, 7720–7725.

12. Shibata,A., Moiani,D., Arvai,A.S., Perry,J., Harding,S.M., Genois,M.M., Maity,R., van Rossum-Fikkert,S., Kertokalio,A., Romoli,F. *et al.* (2014) DNA double-strand break repair pathway choice is directed by distinct MRE11 nuclease activities. *Mol. Cell*, **53**, 7–18.
13. Sartori,A.A., Lukas,C., Coates,J., Mistrik,M., Fu,S., Bartek,J., Baer,R., Lukas,J. and Jackson,S.P. (2007) Human CtIP promotes DNA end resection. *Nature*, **450**, 509–514.
14. Sirbu,B.M. and Cortez,D. (2013) DNA damage response: three levels of DNA repair regulation. *Cold Spring Harb. Perspect. Biol.*, **5**, 1–16.
15. Stewart,G.S., Maser,R.S., Stankovic,T., Bressan,D.A., Kaplan,M.I., Jaspers,N.G., Raams,A., Byrd,P.J., Petrini,J.H. and Taylor,A.M. (1999) The DNA double-strand break repair gene hMRE11 is mutated in individuals with an ataxia-telangiectasia-like disorder. *Cell*, **99**, 577–587.
16. Carney,J.P., Maser,R.S., Olivares,H., Davis,E.M., Le Beau,M., Yates,J.R. 3rd, Hays,L., Morgan,W.F. and Petrini,J.H. (1998) The hMre11/hRad50 protein complex and Nijmegen breakage syndrome: linkage of double-strand break repair to the cellular DNA damage response. *Cell*, **93**, 477–486.
17. Waltes,R., Kalb,R., Gatei,M., Kijas,A.W., Stumm,M., Sobeck,A., Wieland,B., Varon,R., Lerenthal,Y., Lavin,M.F. *et al.* (2009) Human RAD50 deficiency in a Nijmegen breakage syndrome-like disorder. *Am. J. Hum. Genet.*, **84**, 605–616.
18. Mirzoeva,O.K. and Petrini,J.H. (2003) DNA replication-dependent nuclear dynamics of the Mre11 complex. *Mol. Cancer Res.*, **1**, 207–218.
19. Robison,J.G., Elliott,J., Dixon,K. and Oakley,G.G. (2004) Replication protein A and the Mre11.Rad50.Nbs1 complex co-localize and interact at sites of stalled replication forks. *J. Biol. Chem.*, **279**, 34802–34810.
20. Lammens,K., Bemeleit,D.J., Mockel,C., Clausing,E., Schele,A., Hartung,S., Schiller,C.B., Lucas,M., Angermuller,C., Soding,J. *et al.* (2011) The Mre11:Rad50 structure shows an ATP-dependent molecular clamp in DNA double-strand break repair. *Cell*, **145**, 54–66.
21. Cannon,B., Kuhnlein,J., Yang,S.H., Cheng,A., Schindler,D., Stark,J.M., Russell,R. and Paull,T.T. (2013) Visualization of local DNA unwinding by Mre11/Rad50/Nbs1 using single-molecule FRET. *Proc. Natl. Acad. Sci. U.S.A.*, **110**, 18868–18873.
22. Bakkenist,C.J. and Kastan,M.B. (2003) DNA damage activates ATM through intermolecular autophosphorylation and dimer dissociation. *Nature*, **421**, 499–506.
23. Kozlov,S.V., Graham,M.E., Peng,C., Chen,P., Robinson,P.J. and Lavin,M.F. (2006) Involvement of novel autophosphorylation sites in ATM activation. *EMBO J.*, **25**, 3504–3514.
24. Sun,Y., Jiang,X., Chen,S., Fernandes,N. and Price,B.D. (2005) A role for the Tip60 histone acetyltransferase in the acetylation and activation of ATM. *Proc. Natl. Acad. Sci. U.S.A.*, **102**, 13182–13187.
25. Bensimon,A., Aebersold,R. and Shiloh,Y. (2011) Beyond ATM: the protein kinase landscape of the DNA damage response. *FEBS Lett.*, **585**, 1625–1639.
26. Lim,D.S., Kim,S.T., Xu,B., Maser,R.S., Lin,J., Petrini,J.H. and Kastan,M.B. (2000) ATM phosphorylates p95/nbs1 in an S-phase checkpoint pathway. *Nature*, **404**, 613–617.
27. Gatei,M., Jakob,B., Chen,P., Kijas,A.W., Becherel,O.J., Gueven,N., Birrell,G., Lee,J.H., Paull,T.T., Lerenthal,Y. *et al.* (2011) ATM protein-dependent phosphorylation of Rad50 protein regulates DNA repair and cell cycle control. *J. Biol. Chem.*, **286**, 31542–31556.
28. Yazdi,P.T., Wang,Y., Zhao,S., Patel,N., Lee,E.Y. and Qin,J. (2002) SMC1 is a downstream effector in the ATM/NBS1 branch of the human S-phase checkpoint. *Genes Dev.*, **16**, 571–582.
29. Wen,J., Cerosaletti,K., Schultz,K.J., Wright,J.A. and Concannon,P. (2013) NBN phosphorylation regulates the accumulation of MRN and ATM at sites of DNA double-strand breaks. *Oncogene*, **32**, 4448–4456.
30. Gatei,M., Young,D., Cerosaletti,K.M., Desai-Mehta,A., Spring,K., Kozlov,S., Lavin,M.F., Gatti,R.A., Concannon,P. and Khanna,K. (2000) ATM-dependent phosphorylation of nibrin in response to radiation exposure. *Nat. Genet.*, **25**, 115–119.
31. Wu,X., Ranganathan,V., Weisman,D.S., Heine,W.F., Ciccone,D.N., O'Neill,T.B., Crick,K.E., Pierce,K.A., Lane,W.S., Rathbun,G. *et al.* (2000) ATM phosphorylation of Nijmegen breakage syndrome protein is required in a DNA damage response. *Nature*, **405**, 477–482.
32. Matsuoka,S., Ballif,B.A., Smogorzewska,A., McDonald,E.R. 3rd, Hurov,K.E., Luo,J., Bakalarski,C.E., Zhao,Z., Solimini,N., Lerenthal,Y. *et al.* (2007) ATM and ATR substrate analysis reveals extensive protein networks responsive to DNA damage. *Science*, **316**, 1160–1166.
33. Linding,R., Jensen,L.J., Ostheimer,G.J., van,V.M.A., Jorgensen,C., Miron,I.M., Diella,F., Colwill,K., Taylor,L., Elder,K. *et al.* (2007) Systematic discovery of in vivo phosphorylation networks. *Cell*, **129**, 1415–1426.
34. Stokes,M.P., Rush,J., Macneill,J., Ren,J.M., Sprott,K., Nardone,J., Yang,V., Beausoleil,S.A., Gygi,S.P., Livingstone,M. *et al.* (2007) Profiling of UV-induced ATM/ATR signaling pathways. *Proc. Natl. Acad. Sci. U.S.A.*, **104**, 19855–19860.
35. Bennetzen,M.V., Cox,J., Mann,M. and Andersen,J.S. (2012) PhosphoSiteAnalyzer: a bioinformatic platform for deciphering phospho proteomes using kinase predictions retrieved from NetworKIN. *J. Proteome Res.*, **11**, 3480–3486.
36. D'Amours,D. and Jackson,S.P. (2001) The yeast Xrs2 complex functions in S phase checkpoint regulation. *Genes Dev.*, **15**, 2238–2249.
37. Usui,T., Ogawa,H. and Petrini,J.H. (2001) A DNA damage response pathway controlled by Tel1 and the Mre11 complex. *Mol. Cell*, **7**, 1255–1266.
38. Dong,Z., Zhong,Q. and Chen,P.L. (1999) The Nijmegen breakage syndrome protein is essential for Mre11 phosphorylation upon DNA damage. *J. Biol. Chem.*, **274**, 19513–19516.
39. Yuan,S.S., Chang,H.L., Hou,M.F., Chan,T.F., Kao,Y.H., Wu,Y.C. and Su,J.H. (2002) Neocarzinostatin induces Mre11 phosphorylation and focus formation through an ATM- and NBS1-dependent mechanism. *Toxicology*, **177**, 123–130.
40. Di Virgilio,M., Ying,C.Y. and Gautier,J. (2009) PIKK-dependent phosphorylation of Mre11 induces MRN complex inactivation by disassembly from chromatin. *DNA Repair (Amst).*, **8**, 1311–1320.
41. Desai-Mehta,A., Cerosaletti,K.M. and Concannon,P. (2001) Distinct functional domains of nibrin mediate Mre11 binding, focus formation, and nuclear localization. *Mol. Cell. Biol.*, **21**, 2184–2191.
42. Haince,J.F., McDonald,D., Rodrigue,A., Dery,U., Masson,J.Y., Hendzel,M.J. and Poirier,G.G. (2008) PARP1-dependent kinetics of recruitment of MRE11 and NBS1 proteins to multiple DNA damage sites. *J. Biol. Chem.*, **283**, 1197–1208.
43. Jakob,B., Scholz,M. and Taucher-Scholz,G. (2003) Biological imaging of heavy charged-particle tracks. *Radiat. Res.*, **159**, 676–684.
44. Jakob,B., Splinter,J. and Taucher-Scholz,G. (2009) Positional stability of damaged chromatin domains along radiation tracks in mammalian cells. *Radiat. Res.*, **171**, 405–418.
45. Tobias,F., Lob,D., Lengert,N., Durante,M., Drossel,B., Taucher-Scholz,G. and Jakob,B. (2013) Spatiotemporal dynamics of early DNA damage response proteins on complex DNA lesions. *PLoS One*, **8**, e57953.
46. Akyuz,N., Boehden,G.S., Susse,S., Rimek,A., Preuss,U., Scheidtmann,K.H. and Wiesmuller,L. (2002) DNA substrate dependence of p53-mediated regulation of double-strand break repair. *Mol. Cell. Biol.*, **22**, 6306–6317.
47. Lim,Y.C., Roberts,T.L., Day,B.W., Harding,A., Kozlov,S., Kijas,A.W., Ensbey,K.S., Walker,D.G. and Lavin,M.F. (2012) A role for homologous recombination and abnormal cell-cycle progression in radioresistance of glioma-initiating cells. *Mol. Cancer Ther.*, **11**, 1863–1872.
48. Schneider,C.A., Rasband,W.S. and Eliceiri,K.W. (2012) NIH Image to ImageJ: 25 years of image analysis. *Nat. Methods*, **9**, 671–675.
49. Bolderson,E., Tomimatsu,N., Richard,D.J., Boucher,D., Kumar,R., Pandita,T.K., Burma,S. and Khanna,K.K. (2010) Phosphorylation of Exo1 modulates homologous recombination repair of DNA double-strand breaks. *Acids Res.*, **38**, 1821–1831.
50. Zhang,N., Chen,P., Khanna,K.K., Scott,S., Gatei,M., Kozlov,S., Watters,D., Spring,K., Yen,T. and Lavin,M.F. (1997) Isolation of full-length ATM cDNA and correction of the ataxia-telangiectasia cellular phenotype. *Proc. Natl. Acad. Sci. U.S.A.*, **94**, 8021–8026.
51. Wang,Y., Cortez,D., Yazdi,P., Neff,N., Elledge,S.J. and Qin,J. (2000) BASC, a super complex of BRCA1-associated proteins involved in the recognition and repair of aberrant DNA structures. *Genes Dev.*, **14**, 927–939.

52. Kitagawa,R., Bakkenist,C.J., McKinnon,P.J. and Kastan,M.B. (2004) Phosphorylation of SMC1 is a critical downstream event in the ATM-NBS1-BRCA1 pathway. *Genes Dev.*, **18**, 1423–1438.
53. Uziel,T., Lerenthal,Y., Moyal,L., Andegeko,Y., Mittelman,L. and Shiloh,Y. (2003) Requirement of the MRN complex for ATM activation by DNA damage. *EMBO J.*, **22**, 5612–5621.
54. Sanford,K.K., Parshad,R., Price,F.M., Jones,G.M., Tarone,R.E., Eierman,L., Hale,P. and Waldmann,T.A. (1990) Enhanced chromatid damage in blood lymphocytes after G2 phase x irradiation, a marker of the ataxia-telangiectasia gene. *J. Natl. Cancer Inst.*, **82**, 1050–1054.
55. Chen,C., Zhang,L., Huang,N.J., Huang,B. and Kornbluth,S. (2013) Suppression of DNA-damage checkpoint signaling by Rsk-mediated phosphorylation of Mre11. *Proc. Natl. Acad. Sci. U.S.A.*, **110**, 20605–20610.
56. Keimling,M., Volcic,M., Csernok,A., Wieland,B., Dork,T. and Wiesmuller,L. (2011) Functional characterization connects individual patient mutations in ataxia telangiectasia mutated (ATM) with dysfunction of specific DNA double-strand break-repair signaling pathways. *FASEB J.*, **25**, 3849–3860.
57. Beucher,A., Birraux,J., Tchouandong,L., Barton,O., Shibata,A., Conrad,S., Goodarzi,A.A., Krempler,A., Jeggo,P.A. and Lobrich,M. (2009) ATM and Artemis promote homologous recombination of radiation-induced DNA double-strand breaks in G2. *EMBO J.*, **28**, 3413–3427.
58. Morin,I., Ngo,H.P., Greenall,A., Zubko,M.K., Morrice,N. and Lydall,D. (2008) Checkpoint-dependent phosphorylation of Exo1 modulates the DNA damage response. *EMBO J.*, **27**, 2400–2410.
59. Mirzoeva,O.K. and Petrini,J.H. (2001) DNA damage-dependent nuclear dynamics of the Mre11 complex. *Mol. Cell. Biol.*, **21**, 281–288.
60. Zhao,S., Weng,Y.C., Yuan,S.S., Lin,Y.T., Hsu,H.C., Lin,S.C., Gerbino,E., Song,M.H., Zdzienicka,M.Z., Gatti,R.A. *et al.* (2000) Functional link between ataxia-telangiectasia and Nijmegen breakage syndrome gene products. *Nature*, **405**, 473–477.
61. Kim,S.T., Xu,B. and Kastan,M.B. (2002) Involvement of the cohesin protein, Smc1, in Atm-dependent and independent responses to DNA damage. *Genes Dev.*, **16**, 560–570.
62. Bennardo,N., Cheng,A., Huang,N. and Stark,J.M. (2008) Alternative-NHEJ is a mechanistically distinct pathway of mammalian chromosome break repair. *PLoS Genet.*, **4**, e1000110.
63. Tomimatsu,N., Mukherjee,B., Catherine,H.M., Ilcheva,M., Vanessa,C.C., Louise,H.J., Porteus,M., Llorente,B., Khanna,K.K. and Burma,S. (2014) Phosphorylation of EXO1 by CDKs 1 and 2 regulates DNA end resection and repair pathway choice. *Nat. Commun.*, **5**, 1–10.
64. Zhou,Y., Caron,P., Legube,G. and Paull,T.T. (2013) Quantitation of DNA double-strand break resection intermediates in human cells. *Nucleic Acids Res.*, **42**, e19.
65. van den Bosch,M., Bree,R.T. and Lowndes,N.F. (2003) The MRN complex: coordinating and mediating the response to broken chromosomes. *EMBO Rep.*, **4**, 844–849.
66. de Jager,M., van Noort,J., van Gent,D.C., Dekker,C., Kanaar,R. and Wyman,C. (2001) Human Rad50/Mre11 is a flexible complex that can tether DNA ends. *Mol. Cell*, **8**, 1129–1135.